Inorg. Chem. **2006**, *45*, 6612–6621

Bi^{3+}/M^{2+} Oxyphosphate: A Continuous Series of Polycationic Species from the 1D Single Chain to the 2D Planes. Part 2: Crystal Structure of Three Original Structural Types Showing a Combination of New Ribbonlike Polycations

Marie Colmont, Marielle Huvé, and Olivier Mentré*

UCCS, équipe de Chimie du Solide, UMR CNRS 8181, ENSC Lille−UST Lille, BP 90108, 59652 Villeneuve d'Ascq Cedex, France

Received March 1, 2006

With the assistance of structural models deduced from the high-resolution electron microscope (HREM) investigation presented in Part 1 of this work, three new structural types were pointed out in Bi_2O_3–MO–P_2O_5 ternary systems. Their crystal structures are built on the arrangement of 2D polycationic ribbons formed of edge-sharing $O(Bi,M)_4$ tetrahedra and isolated by PO_4 groups. Prior to this study, materials with ribbons up to $n = 3$ tetrahedra wide have been discovered. The original structures presented here display longer $n = 4$–6 cases, which suggests a possible continuous series of polycationic entities that range from the single chain (one tetrahedron wide) to the infinite $[Bi_2O_2]^{2+}$ Aurivillius layer. The ribbons with $n > 3$ show strong structural modifications that are able to bring a good ribbon–phosphate cohesion. In addition to these fascinating structural results, this work fully confirms the validity of the decoding established from HREM images of a single crystallite in inhomogeneous mixtures.

Introduction

In ref 1, henceforth referred to as Part 1, we gave a general description of new double Bi^{3+}/M^{2+} oxyphosphates on the basis of their structure deduction from high-resolution electron microscopy (HREM) images from one single crystallite among multiphased samples. Basically, the investigation of $Bi_2O_3-MO-P_2O_5$ systems has been performed by analogy to the $Bi_2O_3-MO-V_2O_5$ systems, which revealed the existence of the BIMEVOX series,[2] high O^{2-} anionic conductors at medium temperature. The crystal structure of parent compound $Bi_4V_2O_{11}$ belongs to the Aurivillius structural type and can be described by the stacking of $[Bi_2O_2]^{2+}$ and deficient $[VO_{3.5}]^{2-}$ perovskite slabs. The simple observation of the latter as well as the structure of the high temperature δ-Bi_2O_3 (fluorite type) reveals the existence of edge-sharing oxygen-centered OBi_4 tetrahedra arranged into various dimensionalities, e.g., 2D in $[Bi_2O_2]^{2+}$ and 3D in fluorite. This same description applied to the Bi/M oxyphosphate compounds yielded systematic evidence of low-dimensional polycationic species forming the skeleton of structures. $BiMPO_5$ (M = Co, Ni, Mn)[3,4] shows single chains (S). Double ribbons (D), two tetrahedra wide, form the BiM_2PO_6 framework[5−13] and triple ribbons (T) form in $Bi_{\sim 1.2}M_{\sim 1.2}PO_{5.5}$;[14] a mixture of both forms in a number of nonstoichiometric disordered compounds, e.g., $Bi_{\sim 6.2}Cu_{\sim 6.2}P_5O_{28}$,[15]

* To whom correspondence should be addressed. E-mail: mentre@ensc-lille.fr.

(1) The first part of this work: Huvé, M.; Colmont, M. Mentré, O. *Inorg. Chem.* **2006**, *45*, 6604−6611.
(2) Joubert, O.; Jouanneaux, A.; Ganne, M. *J. Mater. Res. Bull.* **1990**, *5*, 2718.
(3) Nadir, S.; Swinnea, J. S.; Steinfink, H. *J. Solid State Chem.* **148**, 295−301.
(4) Abraham, F.; Ketatni, M. *Eur. J. Solid State Inorg. Chem.* **1995**, 429−437.
(5) Huang, J.; Gu, Q.; Sleight, A. W. *J. Solid State Chem.* **1993**, *105*, 599.
(6) Abraham, F.; Ketatni, M.; Mairesse, G.; Mernari, B. *Eur. J. Solid State Chem.* **1994**, *31*, 313.
(7) Tancret, N. Ph.D. dissertation, Université des Sciences et Technologies de Lille, France, 1995.
(8) Mizrahi, A.; Wignacourt, J. P.; Steinfink, H. *J. Solid State Chem.* **1997**, *133*, 516.
(9) Mizrahi, A.; Wignacourt, J. P.; Drache, M.; Conflant, P. *J. Mater. Chem.* **1995**, *5*, 901.
(10) Ketatni, M.; Mernari, B.; Abraham, F.; Mentre, O. *J. Solid State Chem.* **2000**, *153*, 48.
(11) Giraud, S.; Mizrahi, A.; Drache, M.; Conflant, P.; Wignacourt, J. P.; Steinfink, H. *Solid State Sci.* **2001**, *3*, 593.
(12) Abraham, F.; Ketatni, M.; Mernari, B. *Adv. Mater. Res.* **1994**, *1* (2), 223−232.
(13) Xun, X.; Uma, S.; Yokochi A.; Sleight, A. W. *J. Solid State Chem.* **2002**, *167* (1), 245.
(14) Abraham, F.; Cousin, O.; Mentre, O.; Ketatni, M. *J. Solid State Chem.* **2002**, *167*, 168.

10.1021/ic060343j CCC: $33.50
Published on Web 07/25/2006

$Bi_{\sim 3}Cd_{\sim 3.72}M_{\sim 1.28}P_3O_17$ (M = Cu, Co, Zn),[16] $Bi_{\sim 3.785}Cd_{\sim 3.291}Cu_{\sim 1.785}(PO_4)_{3.5}O_{5.5}$.[17] The notion of antistructure on the basis of OM_x frameworks has been known for a long time from the observation of rare earth oxides, oxysalts, and lanthanide salts,[18−22] several disordered systems by O'Keeffe et al.,[23] and, closer to our preoccupation, OPb4 tetrahedra by Krivovichev et al.[24−28] In our case, thanks to the excellent contrast between Bi−M−O polycations and the surrounding PO_4-rich interspace, a HREM image code has been established and fully exploited in complementarity with XRD structural determinations. Ribbons, $n > 3$ tetrahedra wide, mark a further step from isolated polycationic segments toward the infinite $[Bi_2O_2]^{2+}$ planes. Structural proofs of the HREM code versus crystal structure announced in Part 1 then appear necessary for validating the continuous series of polycations in Bi−M−P−O systems. As announced in Part 1, this new image code available for longer cations has been established from the crystal structure of $Bi_{15.32}Cd_{10}(PO_4)_{10}O_{18}$, the first example of sextuplet (six tetrahedra wide) ribbons, called H. This structural investigation is detailed in this work. This paper is also dedicated to the synthesis and investigation of new structural types formed of new polycations ($n > 3$) postulated from the HREM analysis of isolated crystallites in Part 1. We will particularly comment on the structural modifications related to the extension of the size of polycations to $n > 3$.

Experimental Section

Powder Syntheses. Powders have been prepared as already detailed in part 1 of our work.[1] The purity of the samples was checked by powder X-ray diffraction (XRD) using a Siemens D-5000 diffractometer with Cu Kα radiation.

Single Crystal Growth. Single crystals of $Bi_{15.32}Cd_{10}(PO_4)_{10}O_{18}$ have been obtained from the slow cooling (1 °C/h) of a sample of nominal $BiCd_{0.39}P_{0.6}O_{3.29}$ composition after melting it in a gold crucible at 940 °C for 5 h. Colorless crystals corresponding to the new $Bi_{15.32}Cd_{10}(PO_4)_{10}O_{18}$ were extracted from the homogeneous melt.

Single crystals of $Bi_{5.625}Cu_{2.062}(PO_4)_3O_6$ were prepared from a powder of nominal composition $Bi_5Cu_2P_3O_{17}$. The powder was fused at 900° for 5 h and cooled at 2 °C/h. Green needle-shaped crystals were isolated from the melt.

XRD Data Collection. Single-crystal XRD data have been collected on a Bruker SMART CCD 1 K diffractometer under the conditions given in Table 1. The intensities were extracted using the program SaintPlus 6.02.[29] An absorption correction on the basis of the crystal morphology was applied using the program XPREP of the SHELXTL package.[30] Data were re-corrected from the glass fiber and the area detector absorption using empirical corrections with the program SADABS[31] and a null μ_r value. For the two cases presented here, the crystal structure has been solved and refined using the SHELXS direct method option and JANA 2000,[32] respectively.

Elemental Analysis. The EDS (energy dispersive spectroscopy) analysis was performed using a Philips CM30 transmission electron microscope equipped with an energy dispersive spectrometer.

$Bi_{15.32}Cd_{10}(PO_4)_{10}O_{18}$ with the New Dtt/H Structural Type

Synthesis Strategy. First, one should recall the record, already discussed in Part 1, that ruled our goal and synthesis strategy.[1] The ED (electron diffraction) examination of a sample of composition $BiCd_{0.29}Cu_{0.03}P_{0.59}O_{3.29}$ yielded evidence of two new phases with an approximate Bi−Cu−Cd−P formula deduced from EDS analysis and lattice parameters equal to (i) $BiCu_{0.08}Cd_{0.3}P_{0.6}$: a ≈ 11.5 Å, b ≈ 5.5 Å, and c ≈ 21 Å. (ii) $BiCu_{0.03}Cd_{0.2}P_{0.6}$: a ≈ 11.5 Å, b ≈ 5.5 Å, and c ≈ 25 Å. For the former, the HREM image reveals new contrasts by comparison to images for phases containing double and triple ribbons largely studied in prior works.[15−17] To explain the new contrasts, we then provided efforts to reach the concerned structural type. After unfruitful attempts to grow single crystals from either the above mixture or a sample of composition $BiCu_{0.08}Cd_{0.3}P_{0.6}$, a cadmium-only sample with an unchanged Bi^{3+}/M^{2+} ratio was prepared, e.g., composition $BiCd_{0.39}P_{0.6}O_{3.2}$, and led to the studied single crystals by melting and slow-cooling stages described in the Experimental Section.

Structural Refinement. The 8144 reflections ($I > 3\sigma(I)$) are merged in the Laue group *mmm*, R_{int}= 5.41%. The orthorhombic lattice parameters $a = 23.020(4)$ Å, $b = 5.440(1)$ Å, and $c = 20.439(3)$ Å suggest isomorphism to the unknown phase determined from HREM. However, a superstructure involving *a*-doubling occurs. The refinement proceeded in both $Pb2_1m$ and *Pbam* space groups, compatible with the systematic absences. It satisfactorily converged in the centrosymmetric latter group. The [010] zone axis pattern (ZAP) for this new structural type is shown in Figure 1a. The set of systematic extinctions is fully compatible with *Pbam*.

Seven independent heavy Bi−Cd atoms and six oxygens form the ribbon framework. The ratio of the unique mixed Bi/Cd(5) site is refined to 0.33/0.66, which is split over two

(15) Ketatni, M.; Huve, M.; Abraham, F.; Mentre, O. *J. Solid State Chem.* **2003**, *172* (2), 327.
(16) Colmont, M.; Huvé, M.; Ketatni, M.; Abraham, F.; Mentré, O. *J. Solid State Chem.* **2003**, *176* (1), 221.
(17) Colmont, M.; Huvé, M.; Abraham, F.; Mentré, O. *J. Solid State Chem.* **2004**, *177* (11), 4149.
(18) Bergerhoff, G.; Paeslack, J. *Z. Kristallogr.* **1968**, *126*, 112.
(19) Caro, P. E. *J. Less-Common Met.* **1968**, *16*, 367.
(20) Carré, D.; Guittard, M.; Jaulmes, S.; Mazurier, A.; Palazzi, M.; Pardo, M. P.; Laurelle, P.; Flahaut, J. *J. Solid State Chem.* **1984**, *55*, 287.
(21) Schleid, T. *Eur. J. Solid State Inorg. Chem.* **1996**, *33*, 227.
(22) Schleid, T. *Mater. Sci. Forum* **1999**, *163*, 315.
(23) O'Keeffe, M.; Hyde, G. *Struct. Bonding* **1985**, *61*, 77−177.
(24) Krivovichev, S. V.; Filatov, S. K.; Semenova, T. F. *Chem. Rev.* **1967**, *67*, 137.
(25) Krivovichev, S. V.; Filatov, T. F. *Am. Mineral.* **1999**, *84*, 1099.
(26) Krivovichev, S. V.; Armbruster, T.; Depmeier, W. *J. Solid State Chem.* **2004**, *177*, 1321.
(27) Krivovitchev, S. V.; Avdontsva, E. Y.; Burns, P. C. *Z. Anorg. Allg. Chem.* **2004**, *630*, 558.
(28) Krivovitchev, S. V.; Siidra, O. I.; Nazarchuk, E. V.; Burns, P. C.; Depmeier, W. F. *Inorg. Chem.* **2006**, *45*, 3846.
(29) *SAINT+ Area-Detector Integration Software*, version 6.2; Siemens Industrial Automation, Inc.: Madison, WI, 1998.
(30) Sheldrick, G. M. *SHELXTL NT*, version 5.1; Bruker Analytical X-ray Systems: Madison, WI, 1998.
(31) *SADABS Area-Detector Absorption Correction*; Siemens Industrial Automation, Inc.: Madison, WI, 1996.
(32) Petricek, V.; Dusek, M. *JANA 2000*; Institute of Physics: Praha, Czech Republic, 1997.

Table 1. Crystal Data, Measurement, and Structure Refinement Parameters

	$Bi_{15.32}Cd_{10}(PO_4)_{10}O_{18}$	$Bi_{5.625}Cu_{2.062}(PO_4)_3O_6$	$Bi_{20}Cd_{7.42}Cu_{0.58}O_{24}(PO_4)_{12}$
	Crystal Data		
symmetry	orthorhombic	monoclinic	orthorhombic
space group	*Pbam*	$P2_1/m$	*Ibm*2
a (Å)	23.020 (4)	11.592(3)	11.6617(4)
b (Å)	5.4403(09)	5.3227(13)	5.3794(2)
c (Å)	20.439(4)	24.704(6)	25.0587(7)
β (deg)		91.020(5)	
V (Å^3)	2559.7(7)	1526.2(7)	1272.47(5)
Z	2	4	1
	Data Collection		
equipment	Bruker SMART CCD	Bruker SMART CCD	HUBER Guinier G670
radiation type, λ (Å)	Mo Kα, 0.7107	Mo Kα, 0.7107	Cu Kα_1 1.540598
D_{calcd} (g/cm^3)	7.361	7.342	
color	colorless	green	
scan mode	ω	ω	
θ min−max (deg)	2.67−23.29	2.39−28.22	3−50
μ (mm^{-1}) (for λ Kα = 0.7107 Å)	56.94	67.80	
$T_{min}-T_{max}$	0.02704−0.16506	0.01105−0.27755	
T (K)			300
step scan (deg)			0.005
time step (s)			5
R(int) (%)	5.39	9.60	
recording reciprocal space	$-24 \le h \le 24$, $-6 \le k \le 6$, $-22 \le l \le 22$,	$-14 \le h \le 14$, $-6 \le k \le 6$, $-31 \le l \le 31$,	
no. of measured reflns	8144	5702	
no. of ind. reflns. ($I > 3\sigma(I)$)/total	1113/1350	1239/2053	492
limited faces and distances (mm)	0.00 −1.00 0.00 0.2350	0.00 1.00 0.00 0.100	
from an arbitrary origin	0.00 1.00 0.00 0.2350 −1.00 0.00 0.00 0.0220 1.00 0.00 0.00 0.0220 0.00 0.00 −1.00 0.0180 0.00 0.00 1.00 0.0180	0.00 −1.00 0.00 0.100 1.00 0.00 0.00 0.010 −1.00 0.00 0.00 0.010 0.00 0.00 1.00 0.017 0.00 0.00 −1.00 0.017 1.00 −1.00 −7.00 0.055	
	Refinement		
no. of refined params	209	217	67
refinement method, program	L.S. on F, Jana 2000	L.S. on F, Jana 2000	Rietveld, FULLPROF
R1(*F*) [$I > 2\sigma I$]/R1(*F*) [all data] (%)	4.04/5.09	6.35/10.21	
wR2(F^2) [$I > 2\sigma I$]/wR2(F^2) [all data] (%), $w = 1/(\sigma^2)$	10.37/10.86	6.21/7.09	
R_{wp} (%)			17.2
R_p (%)			20.3
R_{Bragg} (%)			8.79
R_F (%)			2.37
χ^2			0.99
zero point			0.0528 (10)
GOF	1.097	1.34	
max., min. residual electron density	2.298, −3.534	11.78, −8.37	
extinction coefficient	0.000057(14)	0.0066(15)	
profile function			pseudo-Voigt, η= 0.849 (7) U = 0.795 (16), V = −0.650(12), W = 0.150 (2)
asymmetry			as1,2 = 0.124 (2), 0.024 (1)

closed 8(i) positions. Three phosphorus molecules and their apexes are located between the ribbons. The P−O distances and O−P−O angle values vary from 1.45(6) to 1.713(5) Å and 94.76(1.8) to 119.91(1.6)°, respectively. It is noteworthy that, compared to the already published "disordered" oxide−phosphate compounds, the observed PO_4 tetrahedra are significantly less disordered and distorted. Two tetrahedral configurations are located around both P(1) and P(2) with 66−33% respective occupancy, in direct relation to their neighboring Bi(5)/Cd(5) cations. However, P(3) shows a single tetrahedral environment, as shown on the Figure 2. Finally, the tunnels (t) whose sections are formed by $P(2)O_4$ and $P(3)O_4$ are occupied by Cd(a) (8(i) site, occupancy = 66%) and Cd(b) ((f) site, occupancy = 34%). A constraint limiting the Cd(a) + Cd(b) mean occupancy of the tunnels was introduced to balance the electroneutrality of the crystal. Results of the refinement are listed in Table 1. Atomic parameters and bond lengths are given in Table 2.

Crystal Structure Description. According to the formalism based on arrangement of $O(Bi,Cd)_4$ in infinite 2D ribbons *n* tetrahedra wide, O(2) and O(3) are at the centers of the tetrahedral interstices of $[Bi_2Cd_4O_4]^{+6}$ double ribbons. O(1), O(4), and O(5) form six-tetrahedra-wide polycations. Compared to ribbons with $n \le 3$, the two central tetrahedra are modified by $O(6)Bi(4)Bi(1)_2Bi(2)_2$ square pyramids growing along the *a* axis. The O(6) oxygen is off-centered from the center of the pyramid basis, e.g., O−Bi = 2 × 2.86(1), 2.43-(4), and 3.37(4) Å. It gives rise to an intermediate pyramidal/tetrahedral character. The sextuplet ribbon formula is $[Bi_{11.34}$-

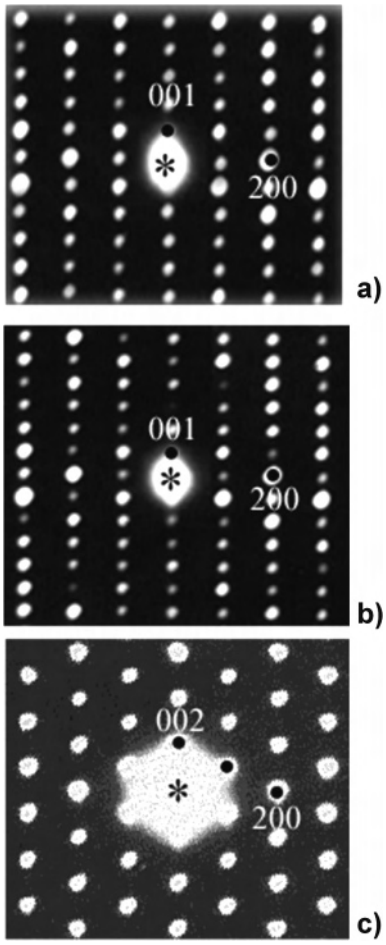

Figure 1. [010] zone axis pattern of (a) H/Qtt, (b) Dtt/H, P⁻ Bravais lattice, and (c) tP/tP, body-centered structural types.

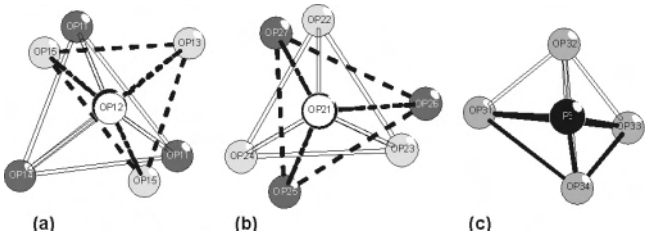

Figure 2. $Bi_{15.32}Cd_{10}(PO_4)_{10}O_{18}$: competition of two tetrahedral configurations around (a) P1 and (b) and P2, and (c) one single O_4 tetrahedron around P3.

$Cd_{2.66}O_{12}]^{+15.34}$. Six and eight PO_4 groups surround double (D) and sextuplet (H) ribbons, respectively. The sequence of this structure can be noted Dtt/H, according to the nomenclature defined in **ref** 33, Figure 3a. As shown in panels b and c of Figure 3, the square pyramid substitutes a PO_4 group with the smallest steric volume, thus enabling a good PO_4−ribbon cohesion.

Tunnel Filling. The Cda and Cdb cations occupy tunnels parallel to the (010) direction. These tunnels are bordered by $P(2)O_4$ and $P(3)O_4$ corners. However, the apparent disorder highlighted by partial occupancies of both Cd(a)/Cd(b) and $P(2)O_4a$/$P(2)O_4b$ may not be so statistical. Therefore, it is noteworthy that the occupancy of the Cd(a)/Cd(b) atoms in the tunnels is related to those of the mixed Bi/Cd(5) sites and the competing phosphate configurations. Thus, according to realistic Cd−O distances and the refined occupancies, it is possible to deduce one and one only ordered Cd(a)/Cd(b) sequence along the tunnel direction. It is shown in Figure 4a and involves ordered [Cd(a)−Cd(a)−Cd(a)−Cd(b)−Cd(a)] segments in three subsequent unit cells with respect the Cd(a)/Cd(b) refined ratio, i.e., Cd(a)/Cd(b) = 1/4. Cd−Cd distances then vary between 2.55(2) and 3.88(1) Å. They are coordinated by 1 $P(3)O_4$, 2/3 $P(2)O_4a$, and 1/3 $P(2)O_4b$. It leads to strongly distorted octahedra around Cd^{2+}, likely for this cation, Table 2.

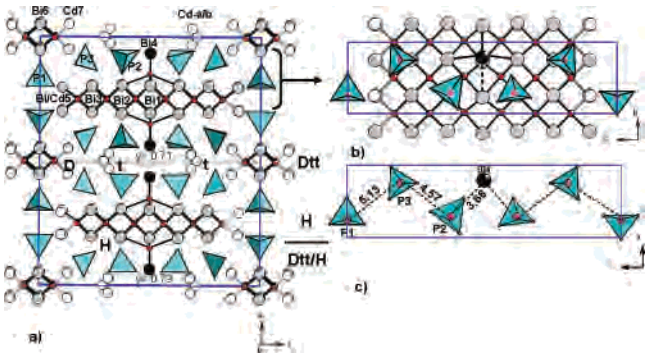

Figure 3. $Bi_{15.32}Cd_{10}(PO_4)_{10}O_{18}$: (a) projection along the (010) direction giving the Dtt/H sequence prominence, (b) view of the square pyramid OBi_5 substituting a PO_4 group, and (c) P−P and P−Bi(4) distances above the ribbon plane.

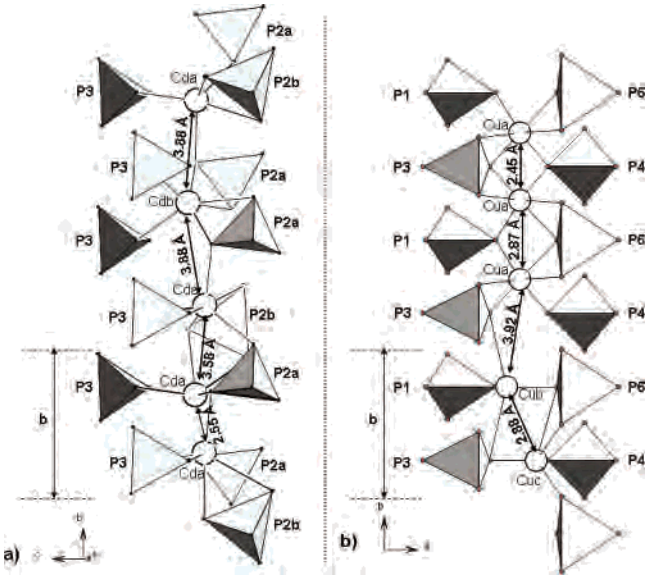

Figure 4. PO_4 surrounding and partial ordering of the tunnels guests. (a) $Bi_{15.32}Cd_{10}(PO_4)_{10}O_{18}$: ideal ordered [Cd(a)−Cd(a)−Cd(a)−Cd(b)−Cd(a)] segments in three subsequent unit cells with respect to the refined occupancies. (b) $Bi_{5.62}Cu_{2.07}(PO_4)_3O_6$: ideal ordered [Cu(c)−Cu(b)−Cu(a)−Cu(a)] fragments along *b*.

***a* Parameter Doubling.** The *a* parameter value is doubled compared to the $a \approx 11.5$ Å value usually observed in these series of compounds. This phenomenon is performed with respect to the *Pbam* symmetry. The combination of the *b* and *a* glides creates D and H images that almost correspond to *a*/2-translated ribbons, i.e., it is due to the particular *x* and/or *y* coordinates of Bi and O. The regular part of the ribbons is then almost unchanged through the unit-cell doubling. This feature is not kept anymore for Bi(6)−O(4)

Table 2. Selected Bond Lengths (Å) for $Bi_{15.32}Cd_{10}(PO_4)_{10}O_{18}$

Intraribbon O−Bi/Cd Bond			
D ribbons		H ribbons	
O(3)−Cd(7)	2 × 2.16(3)	O(1)−Bi(2)	2 × 2.31(2)
O(3)−Bi(6)	2 × 2.27(3)	O(1)−Bi(3)	2 × 2.25(2)
O(2)−Cd(7)	2 × 2.19(3)		
		O(2)−Bi(6)	2 × 2.23(3)
		O(4)−Bi(1)	2 × 2.20(2)
		O(4)−Bi(2)	2 × 2.25(2)
		O(5)−Bi(3)	2 × 2.28(3)
		O(5)−Bi/Cd(5)	2 × 2.23(3)/2.25(3)
		O(6)−Bi(1)	2 × 2.43(4)
		O(6)−Bi(2)	2 × 2.86(2)
		O(6)−Bi(4)	2.01(4)

PO_4 Bonds in Competing Configurations					
P(1)−O		P(2)−O		P(3)−O	
P(1)−Op(11)	1.52(7)	P(2)−Op(21)	1.49(2)	P(3)−Op(31)	1.52(3)
P(1)−Op(11)	1.52(7)	P(2)−Op(22)	1.43(4)	P(3)−Op(32)	1.46(4)
P(1)−Op(14)	1.71(8)	P(2)−Op(23)	1.52(5)	P(3)−Op(33)	1.50(4)
P(1)−Op(12)	1.46(4)	P(2)−Op(24)	1.62(5)	P(3)−Op(34)	1.52(3)
P(1)−Op(12)	1.46(4)	P(2)−Op(21)	1.49(2)		
P(1)−Op(13)	1.48(8)	P(2)−Op(25)	1.56(6)		
P(1)−Op(15)	1.52(6)	P(2)−Op(26)	1.72(7)		
P(1)−Op(15)	1.52(6)	P(2)−Op(27)	1.67(12)		
		P(2)−Op(21)	1.49(2)		

Possible Cd−O in Tunnels					
Cd(a) oct 1		Cd(a) oct 2		Cd(b) oct	
Cd(a)−OP(34)	2.27(3)	Cd(a)−OP(23)	2.35(5)	Cd(b)−OP(23)	2 × 2.06(5)
Cd(a)−OP(25)	2.89(8)	Cd(a)−OP(23)	1.969(5)	Cd(b)−OP(22)	2 × 269(6)
Cd(a)−OP(22)	2.36(6)	Cd(a)−OP(26)	2.51(7)	Cd(b)−OP(34)	2 × 2.34(4)
Cd(a)−OP(23)	2.35(5)	Cd(a)−OP(27)	2.92(2)		
Cd(a)−OP(26)	2.19(7)	Cd(a)−OP(31)	2.68(3)		
Cd(a)−OP(31)	2.68(3)	Cd(a)−OP(34)	2.27(3)		

excrescences that show different *y* altitudes in the two subcells. In the same manner, tunnels and PO_4 are reversed in the next subcell, through the $(1/2 + x, 1/2 - y, z)$ *a* glide symmetry operation. Figure 2a shows pertinent *y* coordinates in the two adjacent subcells.

General Formula. The Dtt/H structural type can be assigned to the general formula: $H_1D_1t_2(PO_4)_{10}$ with H = $Bi_{12}(Bi/M)_4O_{14}$, D = $Bi_4(Bi/M)_4O_4$, t = $M_{x<2}$. As explained in Part 1, the mixed Bi/M positions denote the statistically filled edges of ribbons, whereas the $x < 2$ occupancy denotes the partially M^{2+} filled tunnels under reasonable M−M distances along the *b* axis. So far, it has not been possible to obtain pure powder of this new structural type using a number of M^{2+} cations and variable Bi/M and *x* occupancies. However, the crystal structure refined here is on the basis of the image code establishment reported in Part 1 available for ribbons with $n > 3$.

Verification of the Postulated New H/Qtt Ribbon Sequence in $Bi_{5.62}Cu_{2.07}(PO_4)_3O_6$

Recall and Strategy. In Part 1, in a sample of nominal composition $BiCo_2PO_6$, the presence of a new orthorhombic phase with parameters a ≈ 5.5 Å, b ≈ 11.5 Å, and c ≈ 25 Å was shown by ED. The HREM investigation led to postulating the new H/Qtt structural type, where H, Q, and t stand for six-tetrahedra-wide (hexa) ribbons, four-tetrahedra-wide (quadra) ribbons, and tunnels separated by isolated PO_4 groups, respectively. The deduced mean formula for this new type would be $H_1Q_1t_2(PO_4)_6$, where H = $Bi_{12}(Bi/M)_4O_{14}$, Q = $Bi_8(Bi/M)_4O_{10}$, and t = $M_{x<2}$, leading to $Bi_{20}(Bi,M)_8O_{24}(PO_4)_{12}M_{x<4}$. In the search for structural validation of this model, a great number of compounds with various M^{2+} nature and edges of ribbon and tunnel occupancies have been tested. None show a powder pattern fully indexable with the pertinent unit cell. Finally, single crystals prepared from the heating/controlled cooling of a sample of composition $Bi_{20}Cu_8P_{12}O_{68}$ coincide with this new structural type.

Structural Refinement. After data collection, the 5702 reflections ($I > 3\sigma(I)$) corrected from the absorption were merged in different Laue group symmetries. The symmetry is monoclinic pseudo-orthorhombic (a = 11.591(3) Å, b = 5.3227(13) Å, c = 24.740(6) Å, and β = 91.02 (1)°), but the high value of R_{int} = 9.52% suggests disorder problems and the medium quality of the crystal. The refinement was performed in the $P2_1/m$ space group in good agreement with the ED investigation, Figure 1b.

Fourteen heavy atoms form the ribbon-based framework. Two mixed Bi/Cu(11 and 13) sites have been refined to 0.75(2)/0.25 for an acceptable thermal parameter. Six independent phosphate groups, surprisingly, show a single PO_4 surround-

(33) Huvé, M.; Colmont, M.; Mentré, O. *Chem. Mater.* **2004**, *16* (13), 2628.

Table 3. Selected Bond Lengths (Å) for $Bi_{5.625}Cu_{2.062}(PO_4)_3O_6$

Intraribbon O−Bi/Cu Bond					
Q ribbons		H ribbons			
O(3)−Bi(5)	2.24(4)	O(1)−Bi(1)	2.27(3)	O(4)−Bi(4)	2.30(4)
O(3)−Bi(6)	2 × 2.32(4)	O(1)−Bi(2)	2.29(3)	O(4)−Bi(7)	2.30(4)
2.016(8)	2.26(4)	O(1)−Bi(3)	2 × 2.29(3)	O(4)- Bi(10)	2.15(4)
O(5)−Cu/Bi(11)	2.03(3)	O(2)−Bi(1)	2.32(3)	O(4)- Cu(12)	2.10(4)
O(5)−Cu/Bi(13)	2.02(3)	O(2)−Bi(2)	2.31(3)	O(6)−Bi(1)	2.97(7)
O(5)−Bi(5)	2.32(3)	O(2)−Bi(4)	2.23(3)	O(6)−Bi(2)	2.76(7)
O(5)−Bi(8)	2.23(3)	O(2)−Bi(7)	2.31(3)	O(6)−Bi(3)	2 × 2.86(3)
O(7)−Bi(5)	2.79(5)			O(6)−Bi(14)	1.98(7)
O(7)−Bi(6)	2 × 2.84(2)				
O(7)−Bi(8)	2.97(5)				
O(7)−Bi(9)	2.00(5)				

PO_4 Bonds					
P(1)−O		P(2)−O		P(3)−O	
P(1)−OP(11)	1.45(6)	P(2)−Op(21)	1.45(6)	P(3)−Op(31)	1.51(9)
P(1)−O(12)	1.54(8)	P(2)−Op(22)	1.61(5)	P(3)−Op(32)	2 × 1.60(8)
P(3)−OP(13)	2 × 1.44(4)	P(2)−Op(23)	2 × 1.52(6)	P(3)−Op(32)	1.35(8)
P(4)−O		P(5)−O		P(6)−O	
P(4)−Op(41)	1.60(6)	P(5)−Op(51)	1.51(6)	P(6)−Op(61)	1.60(7)
P(4)−Op(42)	1.41(6)	P(5)−Op(52)	2 × 1.60(4)	P(6)−Op(62)	1.41(10)
P(4)−Op(43)	2 × 1.53(4)	P(5)−Op(53)	1.53(4)	P(6)−Op(63)	2 × 1.53(7)

Possible Cu−O in Tunnels					
Cu(a) octa		Cu(b) tetra		Cu(c) penta	
Cu(a)−OP(12)	2.38(7)	Cu(b)−OP(62)	1.86(2)	Cu(c)−OP(62)	2.77(4)
Cu(a)−OP(62)	2.02(8)	Cu(b)−OP(12)	1.82(9)	Cu(c)−OP(63)	2 × 2.44(2)
Cu(a)−OP(43)	2.09(2)	Cu(b)−OP(33)	2 × 2.73(3)	Cu(c)−OP(33)	1.69(15)
Cu(a)−OP(32)	2.78(1)			Cu(c)−OP(43)	1.77(2)
Cu(a)−OP(33)	1.66(9)				
Cu(a)−OP(63)	266(2)				

ing the tetrahedral configuration. However, one should note that some O−O = 2.7 Å, distance restraints used around P(2) and P(6) to impose a realistic tetrahedral geometry. Cations Cu(a), Cu(b), and Cu(c) have been located in the single independent tunnel. Their occupancies were restrained to balance the electroneutrality of the crystal. As commonly observed for monoclinic structures with β closed to 90°, the introduction of the $hk\bar{l}$ twin law improved the refinement, i.e., ~1% loss in R_1, leading to $R_1 = 6.35\%$. The volumetric crystal 2/crystal 1 ratio is refined to 7.6%/92.4%. Many residual strong peaks (~10 $e^-/Å^3$) subsist on final Fourier difference maps. They are located close to the heavy atoms and suggest bad quality of the crystal, unoptimized absorption corrections, and disorder problems. We have not been able to get a better refinement by changing the absorption corrections or the space group symmetry ($P2_1$, Pm, ...). One should then consider the proposed crystals structure as being imperfect (probably at the level of PO_4 configurations) but certainly showing the true ribbon arrangement and surroundings. Crystal and refinement parameters are listed in Table 1. Atomic positions and bond lengths are reported in Table 3.

Structure Description and Formulation. The crystal structure projected along *b* is shown in Figure 5a. The H/Qtt postulated sequence from the HREM analysis is fully observed. Both sextuplet ribbons (H) and quadruplet ribbons (Q) show fins formed by OBi_5 pyramids. This observation reinforces the critical $n = 3$ tetrahedra wide ribbon value

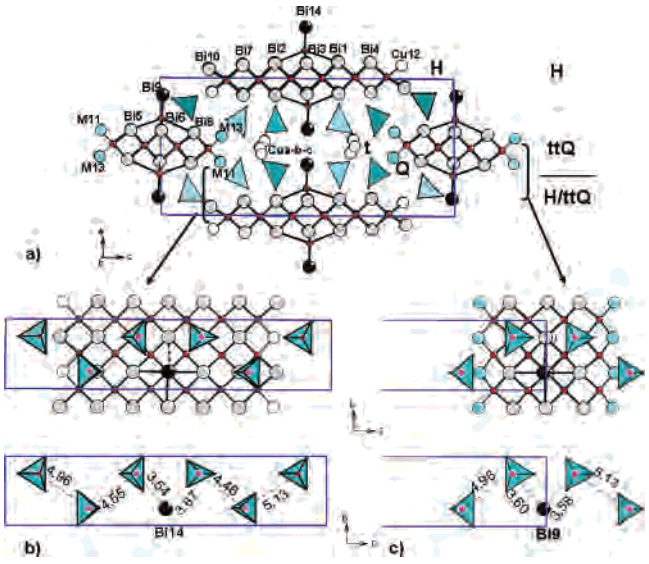

Figure 5. $Bi_{5.625}Cu_{2.062}(PO_4)_3O_6$: (a) projection along the (010) direction giving the H/Qtt sequence prominence; (b and c) Bi(14) substitutes a PO_4 group above H ribbons; (c) Bi(9) substitutes a PO_4 group above Q ribbons.

for their ideal 2D character. As deduced in Part 1 from steric considerations, 12 and eight PO_4 groups surround H and Q, respectively, leading to the general formula $H_1Q_1t_2(PO_4)_6$, where H = $Bi_{12}(Bi/M)_4O_{14}$, Q = $Bi_8(Bi/M)_4O_{10}$, and t = $M_{x<2}$. The mean formula for this new structural type is $Bi_{20}(Bi,M)_8O_{24}(PO_4)_{12}M_{x<4}$. Applied to the investigated crystal,

it becomes H = $[Bi_{14}Cu_2O_{14}]^{+18}$, Q = $[Bi_{11.24}Cu_{0.76}O_{10}]^{+15.24}$, and t = $Cu_{2.2}$ with a slight content excess.

In panels b and c of Figure 5 are shown the PO_4/ribbon fin arrangement with respect to ribbons H and Q. Once more, the substituting role of OBi_5 pyramids for PO_4 is evidenced. Once again, the central oxygen atom is off centered in its Bi_5 environment but significantly less so than in the previous compound. O−Bi distances to the square Bi_4 planes are in the 2.75−2.98 Å range. As performed above in the Dtt/H case, the fine analysis of tunnel content shows possible ordered [Cu(c)−Cu(b)−Cu(a)−Cu(a)] fragments, as shown in Figure 3b. They show Cu−Cu separations between 2.9 and 3.9 Å along the tunnels and Cu coordination between 4 and 6; see Table 3.

Monoclinic Symmetry. The symmetry lowering from orthorhombic to monoclinic is evidenced by the value of β = 91.05(1)°, very close to 90°. The loss of the mirror perpendicular to *c* is mainly due to the OBi_5 fins of the Q and H ribbons that are shifted 0.25 Å *c* out of the pseudomirror (at *z* = 0 and 1/2) planes with respect to the 2_1 helicoidal axis along *b*.

Verification of the New tP/Pt Structural Type

Recall and Synthesis Strategy. First clues of these new structural types have been observed in the sample of composition $BiCd_{0.29}Cu_{0.03}P_{0.59}O_{3.29}$ that contains a mixture of Dtt/H-like compound and at least one unidentified additional phase (orthorhombic *I* lattice, $a \approx 5.5$ Å, $b \approx 11.5$ Å, and $c = 25$ Å). The ED/HREM investigation let us conclude there was a new phase with five-tetrahedra-wide ribbons (P, for penta). Within the hypothesis of a correctly deduced structural model, the mean formula would correspond to $Bi_{20}(Bi,M)_8\ M_{x<4}O_{24}(PO_4)_{12}$, and the isomeric character of the tP/Pt and the H/Qtt structural types has already been noticed. A priori, their isomeric character should not help in the preparation of pure materials. However, the synthesis of the $BiCd_{0.22}Cu_{0.11}P_{0.562}O_{3.24}$ sample led to a powder XRD pattern almost fully indexable using the *I*-centered orthorhombic unit cell, $a = 11.663(8)$ Å, $b = 5.381(5)$ Å, and $c = 25.066(11)$ Å. For the ab initio powder structure determination and Rietveld refinement presented below, only a few unassigned diffraction lines have been excluded from the diagram.

Structure Refinement. The observation of the XRD powder pattern indicates compatible space groups *Ibm*2 or *Ibmm* and agrees well with the previous ED investigation on isomorphous compounds, Figure 1c. However, as strongly suggested by the acentric [010] HREM image and deduced structural arrangement, see Part 1,[1] *Ibm*2 was preferred. After the profile-fitting stage resumed in Table 1, the integrated intensities were used for structure determination using SHELXS. This leads to the localization of seven metal sites that form the ribbons. The mixed nature of the edges of ribbons has been refined on the basis of acceptable thermal parameter values. The phosphorus, oxygen of the ribbons, and Cd atoms of the tunnel guests have been located on subsequent Fourier difference maps. It is noteworthy that our attempts to locate PO_4 corners failed due to disorder problems. Effectively, Fourier difference maps show a number of broad residual peaks around P. This feature is quite commonly observed on these series of compounds, and it has been shown that even neutron diffraction (not available here, because the sample contains strongly absorbing cadmium) is helpless in most of the cases of these series as far as powder diffraction is concerned.[17] Therefore, in the presented results, only the central phosphorus are given. Furthermore, the refined formula is $Bi_{20}Cd_{7.42}Cu_{0.58}O_{24}(PO_4)_{12}$ instead of the prepared $Bi_{20}Cd_{4.4}Cu_{2.2}P_{11.2}O_{65}$ sample. This discrepancy supports the presence of a second minor phase in the sample but also shows the difficulties in refining this kind of disordered crystal structure from powder diffraction data only. At this point, one should remember that the presented model respects the true ribbon-based framework but cannot be considered as being an accurate crystallographic work. The atomic coordinates and distances are listed in Table 4. The observed and calculated diffraction patterns and their differences are shown in Figure 6, conveying a reliable refinement. The projection of the structure is shown in Figure 7.

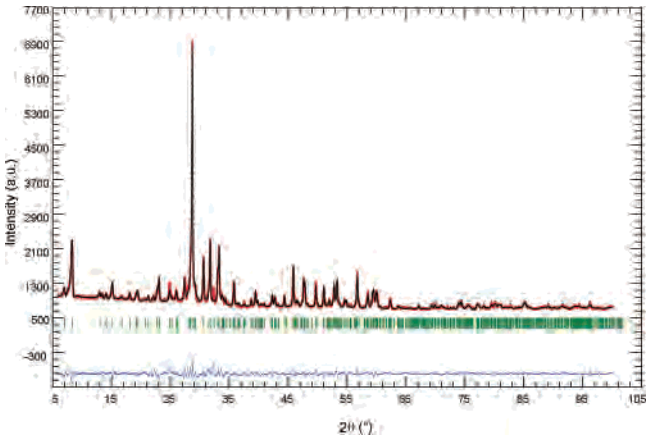

Figure 6. Observed (dots) and calculated (continuous line) XRD patterns and their difference for $Bi_{20}Cd_{7.42}Cu_{0.58}O_{24}(PO_4)_{12}$.

Table 4. Selected Bond Lengths (Å) of P Ribbons in $BiCu_{0.11}Cd_{0.22}(PO_4)_{0.56}O_1$

O(1)−Cd(7)	2 × 2.157(5)	O(2)−Bi(4)	2 × 2.305(6)
O(1)−Bi(4	2 × 2.385(5)	O(2)−Bi(2)	2 × 2.257(8)
O(3)−Bi(2)	2 × 2.490(7)	O(4)−Bi(3)	2 × 2.711(5)
O(3)−Bi(3)	2 × 2.151(3)	O(4)−Bi(5)	2 × 1.939(3)
O(5)−Bi(5)	2 × 2.03(3)	O(6)−Bi(2)	3.285(4)
O(5)−Cd(9)	2 × 2.03(3)	O(6)−Bi(3)	2.998(1)
		O(6)−Bi(5)	2.714(1)
		O(6)−Bi(6)	1.786(3)

Discussion

As mentioned in the Introduction, several chemical systems based on rare earth, lanthanides, or other metals are very convenient for a structural description on the basis of oxo-centered OM_4 tetrahedra assemblies in various edifices. For instance, it has been shown that this concept is very convenient for clearly viewing the relationships between the α-, *β*-, and recent *ϵ*-Bi2O3 polymorphs through the reorganization of infinite $[Bi_2O_3]$ single chains formed of OBi_4

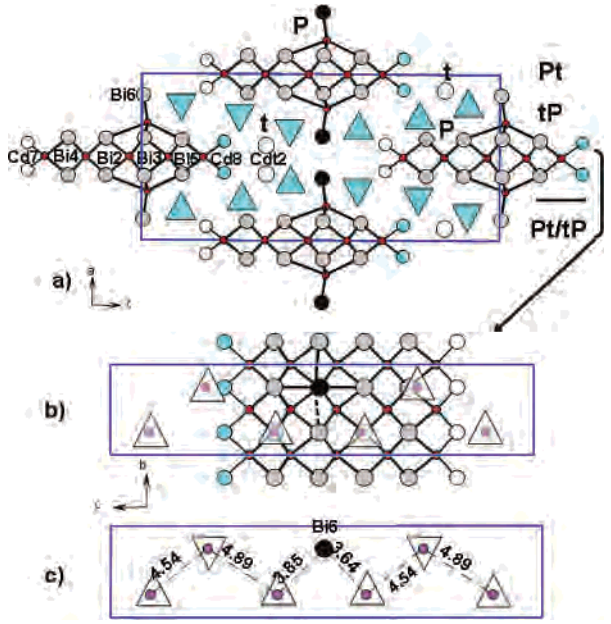

Figure 7. $Bi_{20}Cd_{7.42}Cu_{0.58}O_{24}(PO_4)_{12}$: (a) projection along the (010) direction giving the tP/tP sequence prominence. The PO_4 orientation is assumed from the central P refined positions; (b) Bi(6) substitutes a PO_4 group; (c) P−P and P−Bi distances above the ribbon plane.

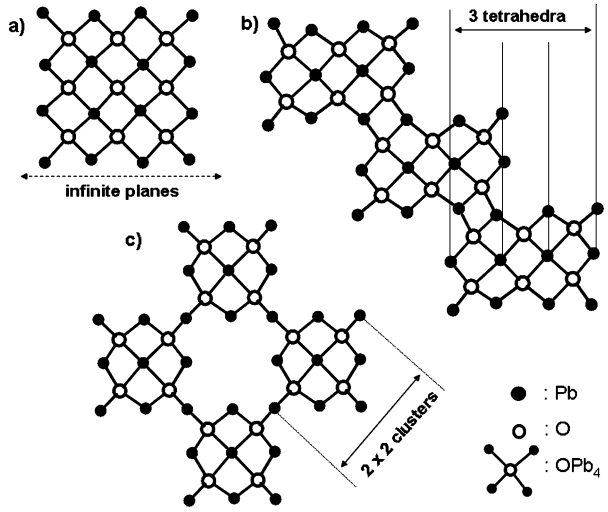

Figure 8. Different lacunar sheets of oxo-centered OPb_4 tetrahedra that form (a) filled [PbO] layers in the tetragonal PbO, (b) Cresnel-like ribbons, three-tetrahedra-wide $Pb_5O_4(CrO_4)$, and (c) corner-sharing clusters of 2 × 2 tetrahedra surrounded by vacancies in $Pb_8O_5(AsO_4)_2$.

edge-sharing tetrahedra.[34] In the case of Pb^{2+}, it is isoelectronic with Bi^{3+}. Lead oxide salts are usually described in terms of 1D−2D edifices on the basis of the linkage of OPb_4 units. These structural blocks can be considered as being derivates from [PbO] layers found in the tetragonal PbO form, in which the layers are separated by ∼5 Å, which corresponds to the 4-fold axis. Krivovichev et al.[24−27] described the existing sheets in an elegant way on the basis of the lattice of black (OM_4 filled space) and white squares (lattice vacancies). A number of arrangements then exist and are rapidly distinguished. They range from fully occupied $[PbO]/[Bi_2O_2]^{2+}$-like sheets in tetragonal PbO to $[Bi_2O_2](A_{n-1}B_nO_{3n+1})$ Aurivillius phases (for a more exhaustive list, see ref 26) and lacunar sheets with a number of possible arrangements. Figure 8 shows the lacunar sheets of oxo-centered OPb_4 tetrahedra, which form Cresnel-like ribbons, three-tetrahedra-wide $Pb_5O_4(CrO_4)$, and clusters of 2 × 2 tetrahedra surrounded by vacancies in $Pb_8O_5(AsO_4)_2$ by comparison to filled [PbO] layers in the tetragonal PbO. Within the series of OM_4-based infinite chains, which are reported in the literature with M ≠ Bi, one should note $[Pb_2O]^{2+}$ single chains in $Pb_2O(XO_4)$, X = S,[35] Cr,[36] Mo,[37] W,[38]..., $[Pb_3O_2]^{2+}$ double chains in $Pb_3O(X)_2$, X = I,[39] Cl,[40] OH,[41] Br, [42] ..., and triple $[La_4O_3]^{6+}$ in $La_4O_3(AsS_3)$[43]... but no evidence of infinite ribbons of greater width is reported, which reinforces the innovative interest of the three new compounds. The continuous evolution of $Bi^{3+}/M^{2+}/O^{2-}$ polycationic ribbons from the 1D chains of edge-sharing tetrahedra toward 2D ribbons of variable width (n = 2 (D), 3 (T) tetrahedra wide) is then reinforced by the finding in this work of n = 4 (Q), 5 (P), and 6 (H) units. Considering the number of possible arrangements of these ribbons, polycations should be considered as being building units that may arrange together through PO_4 surroundings. The nomenclature that we defined[15−17,23] pictures rather well this associating aspect, e.g., H/Qtt pictures the combination of H and Q ribbons isolated by PO_4 groups that creates two tunnels between two Q. Considering the whole series of materials of this type discovered so far, the common structural features of ribbons is the systematic Bi^{3+}-only nature of the central cationic positions and the mixed Bi^{3+}/M^{2+} nature of the edges of ribbons responsible for the disorder over several PO_4 configurations around them. The $O(Bi/M)_4$ tetrahedra are rather regular with O−metal distances between 2 and 2.5 Å. However, we have shown here that the perfect compatibility of $n \leq 3$ ribbons with a PO_4 surrounding is largely broken when $n > 3$. Effectively, for these, the 2D shape is modified by the appearing of so-called fins formed by OBi_5 pyramids. Until the n = 3 critical size, the coordination of both Bi^{3+} and M^{2+} by PO_4 corners is enabled, whereas the substitution of one PO_4^{3-} by a smaller $[Bi-O]^+$ block is necessary with respect to correct Bi−O and M−O distances. Polycations can be formulated as $[(Bi/M)_4Bi_{2n-2}O_{2n}]^{x+}$ until n = 3; they then become $[(Bi/M)_4Bi_{2n}O_{2n+2}]^{y+}$ for greater $3 < n < 7$ values. These general formulations of ribbons form the first stages of a rationalization of the chemical composition applicable to the full series. The predicting and designing of new compounds is highly attractive when applied to the studied systems. It has already

(34) Cornei, N.; Tancret, N.; Abraham, A.; Mentré, O. *Inorg. Chem.* **2006**, 45, 4886−4888.
(35) Sahl, K. *Z. Kristallogr.* **1970**, *132*, 99.
(36) Williams, S. A.; Mc. Lean, W. J.; Anthony, J. W. *Am. Mineral.* **1970**, *55*, 784.
(37) Mentzen, B. F.; Latrach, A.; Bouix, J.; Hewat, A. W. *Mater. Res. Bull.* **1984**, *19*, 549.
(38) Bosselet, F.; Mentzen, B. W.; Bouix, J. *Mater. Res. Bull.* **1985**, *20*, 1329.
(39) Kramer, V.; Post, E. *Mater. Res. Bull.* **1985**, *20*, 407.
(40) Vincent, H.; Perrault, G. *Bull. Soc. Fr. Miner. Cristallogr.* **1971**, *94*, 323.
(41) Krivovichev, S. V.; Burns, P. C. *Eur. J. Mineral.* **2001**, *13*, 801.
(42) Krivovichev, S. V.; Burns, P. C. *Solid State Sci.* **2001**, *3*, 455.
(43) Palazzi, M.; Jaulmes, S. *Acta Crystallogr., Sect. B* **1981**, *37*, 1340.

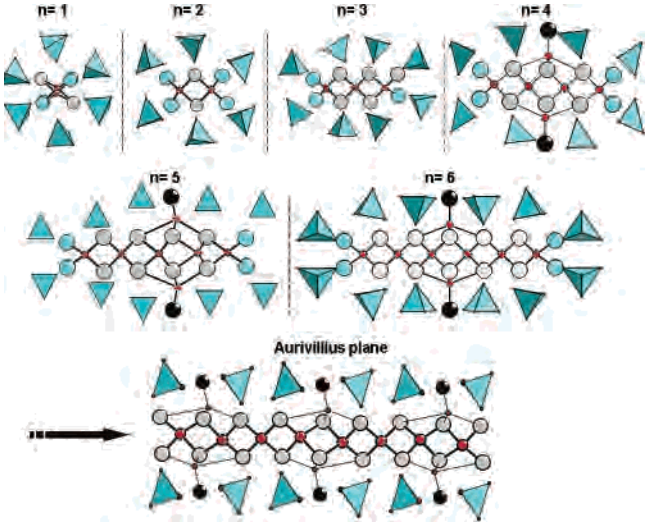

Figure 9. Different kinds of ribbons, from the single chain, $n = 1$ O(Bi/M)$_4$ tetrahedron wide, to infinite layers.

been successfully applied on the basis of the fruitful concept of building blocks. For instance, inorganic skeletons of porous materials can be designed using a predictive manner to assemble building units,[44−46] or new inorganic compounds can be designed from 2D building blocks of fluorite and antifluorite type.[47] In our case, it is easily possible to design potential new materials from the association of ribbons, phosphates, and tunnels; the constraining parameters are the geometrical matching ruled by well-known parameters such as the number of PO_4 around each kind of ribbon, whether the tunnel is possible or not, and localization at the center of the four phosphate groups. However, considering the number of available blocks, it seems difficult to generalize a unified process and each case should be treated on its own merit. The various terms isolated to date are shown in Figure 9.

It is obvious that the infinite n extension of ideal ribbons leads to the $[Bi_2O_2]^{2+}$ Aurivillius-like layers. However, they are not commonly found sandwiched between layers of isolated tetrahedra, but in perovskite slabs in Aurivilius compounds, edge-sharing compact tetrahedral sheets in BiOCuSe,[48] or isolated between small anions in Sillen compounds, e.g., Cl^- in BiOCl[49] or OH^-/NO_3^- in $Bi_2O_2(OH)NO_3$.[50]

However, it is known that the $Bi_4V_2O_{10.66}$ compound obtained by H_2/N_2 reduction of $Bi_4V_2O_{11}$ shows rearrangement of $[VO_{3.5}]^{2-}$ perovskite layers into $[VO_{3.33}]^{2+}$ slabs with segregated $V^{5+}O_4$ tetrahedra and $V^{4+}O_6$ octahedra. As shown

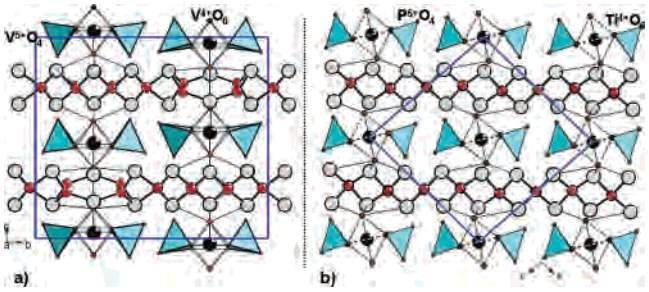

Figure 10. Structural analogy between (a) $Bi_4V_2O_{10.66}$ and (b) $Bi_6TiP_2O_{16}$ layers; $[Bi_2O_2]^{2+}$ infinite layers surrounding by (a) $V^{4+}O_6$ and $V^{5+}O_4$ or (b) $Ti^{4+}O_6$ and $P^{5+}O_4$.

on the Figure 10a, its crystal structure shows the first example of the $n \rightarrow \infty$ extension of the polycationic species, n tetrahedra wide, where V^{4+} octahedra play the role of the fins periodically (every three tetrahedra) on the ribbons. However, during the reduction process, the $[Bi_2O_2]^{2+}$ layers are slightly modified by oxygen displacements, and a closer model can be found in the recently published $Bi_6TiP_2O_{16}$ that exhibits the same basic framework but is less distorted. It is shown in Figure 10b. In this compound, $[Bi_2O_2]^{2+}$ slabs are sandwiched between $[TiP_2O_{16}]$ layers with corner-sharing PO_4 and TiO_6 polyhedra. The apical TiO_6 corners play the role of the central OBi_5 anions in Q, P, and H, whereas Ti plays the role of the extra Bi found in ribbon fins. Once more, one TiO_6 and two PO_4 alternate along the ribbon dimension, confirming the probable systematic modification of ribbons for every $n > 3$ value, Figure 10.

Concluding Remarks

The work presented here should not be considered as the report of only three new structural types in the $Bi_2O_3-P_2O_5-$MO system for the reasons detailed here. First, the Dtt/H crystal structure determination has pointed out the existence of the new H bidimensional polycationic species formed of $n = 6$ edge-sharing O(Bi,M)$_4$ tetrahedra. It strongly suggests the existence of a continuous series of polycations from $n = 1$ to ∞ tetrahedra wide, although only $n = 1-3$ terms have been described in previous works. In H, strong structural modifications of the ribbon structure have been highlighted compared to prior studies limited to $n = 3$. This result, explained on its own the strong modification of the HREM contrasts observed on new unknown materials and, with the help of the Dtt/H crystal structure, it has been possible to establish an image code for $n > 3$. It thus enables us to predict−formulate−synthesize−verify both H/Qtt and tP/Pt new types from the HREM photographs of isolated crystallites in mixtures. By comparison to S ($n = 1$ tetrahedron wide), D ($n = 2$), and T ($n = 3$) ribbon structures, the modification of the ribbons appears to be systematic for $n > 3$, i.e., Q ($n = 4$), P ($n = 5$) and H ($n = 6$); all show OBi_5 excrescences pointing toward the PO_4 surrounding for a good structural cohesion. This feature should be conserved for hypothetical $n > 6$ ribbons, because comparable modifications are observed on the $[Bi_2O_2]^{2+}$ infinite planes surrounding phosphates in $Bi_6TiP_2O_{16}$. Finally, considering the number of polycation arrangements among the series of Bi^{3+}/

(44) Ferey, G. *J. Solid State Chem.* **2000**, *152*, 37.
(45) Yaghi, O. M.; O'Keefe, M.; Ockwig, N. W.; Chae, H. K.; Eddaoudi, M.; Kim, J. *Nature* **2003**, *423*, 705.
(46) Mellot-Draznieks, C.; Ferey, G. *Curr. Opin. Solid State Mater. Sci.* **2003**, *7*, 13.
(47) Cario, L.; Kabbour, H.; Meerschaut, A. *Chem. Mater.* **2005**, *17*, 234−236.
(48) Kusainova, A. M.; Berdonosov, P. S.; Akselrud, L. G.; Kholodkovskaya, L. N.; Dolgikh, V. A.; Popovkin, B. A. *J. Solid-State Circuits* **2002** *112*, 189−191.
(49) Keramidas, K. G.; Voutsas, G. P.; Rentzeperis, P. I. *Z. Kristallogr.* **1993**, *204*, 40.
(50) Henry, N.; Evain, M; Deniard, P.; Jobic, S.; Mentre, O. Abraham, F. *J. Solid State Chem.* **2003**, *176* (1), 126−136.

M^{2+} oxophosphates, the self-building-unit role of the ribbons is highlighted, which is theoretically the basis of the suggestion of an unlimited number of new compounds.

Acknowledgment. M.C. thanks the Région-Nord-Pas-de-Calais for financial support. The Fonds Européen de Développement Régional (FEDER), CNRS, Région Nord Pas-de-Calais, and Ministère de l'Education Nationale de l'Enseignement Supérieur et de la Recherche are acknowledged for funding of X-ray diffractometers.

Supporting Information Available: Complementary crystallographic data and CIF files. This material is available free of charge via the Internet at http://pubs.acs.org.

IC060343J